ISSN 0003-701X, Applied Solar Energy, 2024, Vol. 60, No. 1, pp. 83–89. © Allerton Press, Inc., 2024.

SOLAR ENERGY CONCENTRATORS

Uniform Side-Pumping of Solar Solid-State Laser Based on Fresnel Lens Array

Hongfei Qi[a], Yan Liu[a, *], Lanling Lan[a], Yuanyuan Zhang[a], and Xiuhua Ma[b]

[a] *Center for Astronomy and Space Science, College of Science, China Three Gorges University, Yichang, Hubei, 443002 China*

[b] *Shanghai Institute of Optics and Fine Mechanics, Chinese Academy of Sciences, Shanghai, 201800 China*

**e-mail: liuyan703@163.com*

Received August 23, 2023; revised November 24, 2023; accepted January 18, 2024

Abstract—Uniform side-pumping can reduce the thermal stress of laser crystal rod and is an effective method to achieve high power laser output. In order to realize the uniform side-pumping of the laser crystal rod, a solar concentrating system based on plane mirrors and linear Fresnel lens array is proposed. Rays tracing shows that the concentrating efficiency of solar concentrating system and the uniformity of the light spot reach 66.5 and 98.5% with optimization. The temperature distribution in the laser crystal rod is calculated by Comsol software. The results show the central temperature and the surface temperature of laser rod are 316 and 306 K, respectively. Base on solving the rate equations, the laser output characteristics are analyzed. The laser output power and the solar-to-laser conversion efficiency are 88.5 W and 3.3%, respectively. This uniform side-pumping configuration provides the new method for developing high power solar-pumped solid-state lasers.

Keywords: solar-pumped laser, plane mirror, linear Fresnel lens, uniform side-pumping

DOI: 10.3103/S0003701X23601333

INTRODUCTION

Solar-pumped lasers can directly convert solar energy into laser, which is one of the direct utilization ways of solar energy. Nowadays, the research of solar-pumped lasers has attracted a lot of attention. Solar-pumped lasers have great applications prospects in wireless power transmission, laser communication, and energy utilization [1–4].

The laser output of solar-pumped laser was first realized by experiment in 1963 [5]. Since then, the development of solar-pumped lasers has made great progress. Improving the output power, solar-to-laser conversion efficiency and laser beam quality is the development goal of solar laser [6–9]. The pumping methods of solar solid-state lasers can be divided into end-pumping and side-pumping. In end-pumping, the pump light propagates along the axial direction of the laser crystal, and a high pumping efficiency can be obtained. But serious thermal effects will be produced due to the inability to achieve uniform absorption of the pump light, which will worsen the laser beam quality and eventually limit the laser output power. In 1975, J. Falk used a reflecting telescope system as solar concentrator to end-pump the laser crystal and obtained a laser output of 5.6 W [10]. In 1992, D. Cooke also used a reflecting telescope system for solar end-pumping of Nd:YAG and Nd:Cr:GSGG, and obtained laser outputs of 1.7 and 3.2 W, respectively [11]. In 2007, T. Yabe used a Fresnel lens for end-pumping of Cr:Nd:YAG and obtained a laser output of 24.4 W [12]. In 2021, M. Ou designed a new Fresnel lens for end-pumping of Nd:YAG, and this hybrid Fresnel lens achieves a concentrating efficiency of 73.2% at the end face of laser crystal with a radius of 3 mm [13]. Compared with the end-pumping, the pump area of the side-pumping increases considerably and uniform absorption of the pumped light can be achieved, which can reduce the associated thermal loading problems, and improve the beam quality and laser output power [14–16]. In 2003, M. Lando obtained a laser output of 45 W by solar side-pumping Nd:YAG (Φ 6 × 72 mm) [17]. In 2012, T.H. Dinh obtained a laser output of 120 W by using a Fresnel lens and a conical cavity as solar concentrator for end-side-pumping of Nd:YAG [18]. In 2014, C. Zhao obtained a laser output of 27 W by using end-side pumping method [19]. In 2015, D. Liang obtained a laser output of 5.5 W TEM_{00} mode with a side pumping method [20]. In 2017, they used twisted light-guide to achieve the laser crystal rod uniform pumping of the sunlight and finally obtained a TEM_{00} mode output power of 2.7 W [21]. In 2020, a 32 W TEM_{00}-mode side-pumped solar laser was demonstrated based on parabolic mirror, rectangular hollow pipe and 2V-shaped dry pump cavity [22]. In 2021, four off-axis parabolic mirrors acted as concentrator to achieve side-pumping

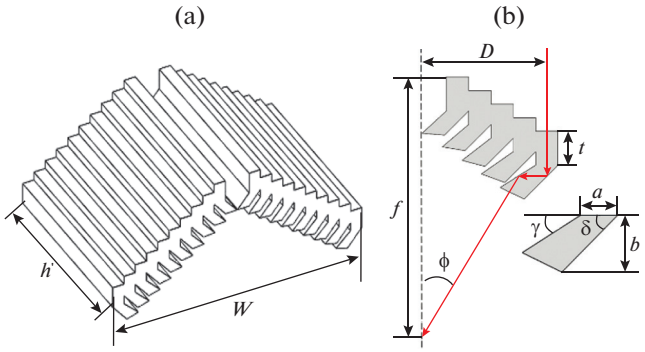

Fig. 1. Schematic diagram of linear Fresnel lens structure (a) and Fresnel lens focusing principle (b).

of the Nd:YAG (Φ 7.5 × 84 mm), and laser output of 346.8 W was obtained [23]. In order to overcome the low launching power, side-pumping method is also used for the solar rare-doped fiber laser [24, 25] and solar single crystal fiber laser [26].

In recent years, because the absorption spectrum of Ce:Nd:YAG has high overlop over the sunlight spectrum, it is acted as the gain medium to improving the efficiency of solar pumped lasers. In 2021, C. Vistas reported a solar pumped Ce:Nd:YAG laser [27]. When the incoming solar power was 600 W, the collection efficiency, solar-to-laser efficiency and slope efficiency were 23.6 W/m^2, 2.8 and 4.4%, respectively. In 2022, J. Almeida used Ce:Nd:YAG as the gain medium for a solar pumped laser [28], and the continuous laser output and the slope efficiency were 40W and 2.44%, respectively. In the same year, D. Garcia conducted end-side pumping experiments on Ce:Nd:YAG using sunlight [29], and the continuous laser output reached 11.2 W and solar-to-laser efficiency was 4.5%. D. Liang demonstrated a solar pumped Cr:Nd:YAG laser with output power of 16.5 W, and the solar-to-laser conversion efficiency and collection efficiency reached 4.64% and 41.25 W/m^2 [30]. In 2023, Z. Cai also conducted solar side pumping experiments on Ce:Nd:YAG [31], and 26.93 W laser output was obtained with a slope efficiency of 6.33% and a collection efficiency of 38.8 W/m^2.

To obtain high power laser output and good beam quality, side-pumping is the preferred pumping method. Side-pumping makes it easier to collect the sunlight on the laser crystal surface, and the sunlight can be uniformly distributed along the axial direction of laser crystal, which can reduce the thermal load on the laser crystal rod. Therefore, a new concentrating system is developed for solar side-pumping based on the combination of a plane mirror and a linear Fresnel lens. Compared with the side-pumping method with multiple linear Fresnel lens in [32], the difference are as follows: (1) The sunlight focused by the Fresnel lenses on two ends of gain medium can compensate for each other; (2) the Fresnel lens are optimized to make the sunlight converging on the laser crystal rod uniformly; (3) The concentrator system proposed in this paper does not require the use of a spherical lens to further compress the focused spot of the linear Fresnel lenses, and the design of the laser head is simplified. The simulation shows that sunlight can be uniformly distributed on the laser crystal surface (66.5% of concentration efficiency and 98.5% of uniformity), which can provide a design of a solar concentrating system for high power solar-pumped laser.

ESIGN OF THE SOLAR CONCENTRATING SYSTEM

Design of Sub-Concentration System

The whole concentrating system consists of an array of plane mirrors and linear Fresnel lenses. Each subsystem consists of seven linear Fresnel lenses and seven plane mirrors. The incident sunlight is reflected by the plane mirrors and is incident vertically on the surface of the liner Fresnel lens. In order to improve the concentrating efficiency, the Fresnel lens uses a new type of twice total internal reflection Fresnel lens [13], whose structure is shown in Fig. 1. The focal length f of the Fresnel lens is 1050 mm, and D indicates the distance from each prism of the Fresnel lens to the central axis. The thickness t of the Fresnel lens is 1.5 mm and the width a of the prism is 0.33 mm. The angle δ between the outer edge of the prism and the horizontal direction is 45°, and h' is the height of linear Fresnel lens.

Figure 2 shows the schematic diagram of a solar concentrating sub-system. In the subsystem, the middle linear Fresnel lens is called as F_0. The linear Fresnel lens above F_0 are F_1, F_2 and F_3, and below F_0 are F_{-1}, F_{-2} and F_{-3}, respectively. The linear Fresnel lenses F_1, F_2, F_3, and the linear Fresnel lenses F_{-1}, F_{-2}, F_{-3} are symmetrically distributed to the linear Fresnel lens F_0. The laser crystal rod (Φ 6 × 100 mm) is Nd:YAG and placed at the focal point of the linear Fresnel lens F_0. The length of the laser crystal rod is the same as the height of the linear Fresnel lens. In order to let the sunlight pass through the linear Fresnel lens and converge on the side of the laser crystal rod, the linear Fresnel lens except F_0 should be tilted at a certain angle, which can make the converge sunlight of the linear Fresnel lens besides F_0 complement each other and achieve the uniform distribution of solar power on the laser rod.

In Fig. 2, β_i is the included angle of the plane mirror in the vertical direction, and l_i is the vertical distance from the lower edge of the plane mirror M_i to the lower edge of the plane mirror M_0. x_i is the horizontal distance from the lower edge of the plane mirror M_i to the linear Fresnel lens F_i, H_i is the vertical distance from the center of the linear Fresnel lens F_i to the center of the linear Fresnel lens F_0, and h_i is the distance

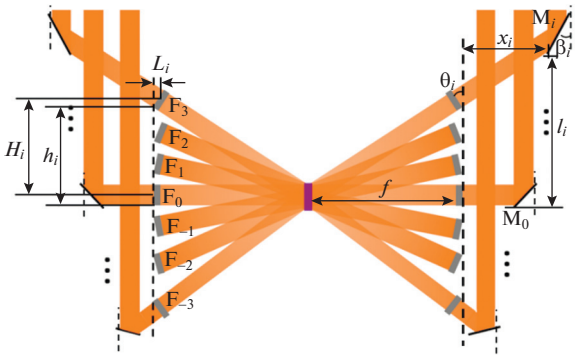

Fig. 2. Schematic diagram of a solar concentrating subsystem.

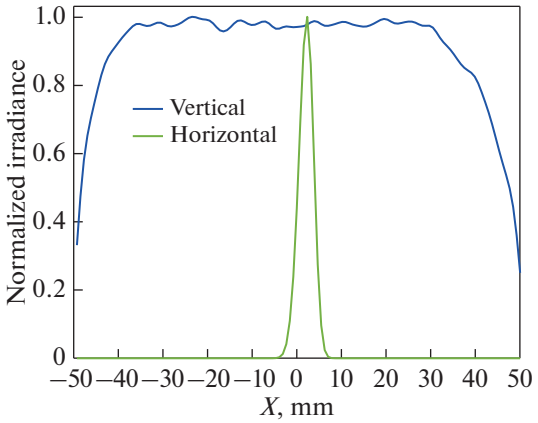

Fig. 3. Irradiance map of crystal rod side.

from the lower edge of the linear Fresnel lens F_i to the lower edge of the linear Fresnel lens F_0. θ_i is the tilt angle of the linear Fresnel lens F_i in the vertical direction, and f is the focal length of linear Fresnel lens F_0. Since the Fresnel lenses F_1, F_2, F_3 and the Fresnel lenses F_{-1}, F_{-2}, F_{-3} are symmetric to the Fresnel lens F_0. Only the positions of the Fresnel lenses F_1, F_2 and F_3 need to be calculated. The following equations can be obtained according to the geometric relationship of Fig. 2.

$$L_i = \frac{h'}{2}\sin\theta_i, \tag{1}$$

$$H_i = (f - L_i)\tan\theta_i, \tag{2}$$

$$h_i = H_i - \frac{h'}{2}\cos\theta_i + \frac{h'}{2}. \tag{3}$$

In order to obtain the Fresnel lenses without rays blockage, the tilt angle θ_{i+1} of the Fresnel lens can be obtained as following.

$$\tan\theta_i = \frac{H_i - \frac{h'}{2}\cos\theta_i + h'\cos\theta_i + \frac{h'}{2}\cos\theta_{i+1}}{f - h'\sin\theta_i - \frac{h'}{2}\sin\theta_{i+1}}. \tag{4}$$

For given the angle θ_1, the positions of the other linear Fresnel lenses can be obtained according to (4). The focal length f, the height h' and the width W of linear Fresnel lens F_0 are taken as 1050, 100 and 648 mm, respectively. When the tilt angle θ_1 of linear Fresnel lens F_1 is 10°, through the expression (1)–(4), we can get $h_1 = 179$ mm, $\theta_2 = 15.6°$, and $h_2 = 279.1$ mm, $\theta_3 = 21.1°$, $h_3 = 385.7$ mm. Meanwhile, the geometric relationship can be obtained from Fig. 2. If the values of θ_i, h_i and x_i are given, the position of each plane reflector can be obtained based on (5), (6).

$$\beta_i = 45° - \frac{\theta_i}{2}, \tag{5}$$

$$l_i = h_i + x_i\tan\beta_i. \tag{6}$$

Design of Laser Head

The laser head consists of the laser crystal rod, the cooling water and the quartz tube. The laser head is placed at the focal point of the linear Fresnel lens F_0. The radius of laser crystal rod, the radius of cooling water channel and thickness of quartz tube are 3, 4.5 and 1 mm, respectively.

With TracePro software, the concentrating effect of the solar concentrating system can be analyzed by ray tracing. In the simulation, two parameters of the concentrating efficiency and uniformity of light spot are defined. The ratio of the irradiance flux (φ_{out}) at the output face to the irradiance flux (φ_{in}) at the input face is called the concentrating efficiency, i.e.

$$\eta_0 = \frac{\phi_{out}}{\phi_{in}} \times 100\%. \tag{7}$$

The uniformity of irradiance on the receiving surface is expressed as [33]

$$\Delta E = \left(1 - \frac{E_{max} - E_{ave}}{E_{max} + E_{ave}}\right) \times 100\%. \tag{8}$$

Here, E_{max} and E_{ave} are the maximum irradiance and the average irradiance on the receiving surface, respectively. The irradiance of crystal rod side was shown in Fig. 3. When the power density of sunlight is taken as 900 W/m^2 [34], the concentrating efficiency and uniformity are 63.5 and 96%. It is found that the laser crystal rod has high power density of sunlight in the middle of laser rod and low power density at the two ends, which will cause a serious thermal effect of the laser crystal rod.

OPTIMIZATION OF THE CONCENTRATING SYSTEM

In order to solve the problem of high solar power density of in the middle of the laser crystal rod and low at both ends. Each linear Fresnel lens is divided into

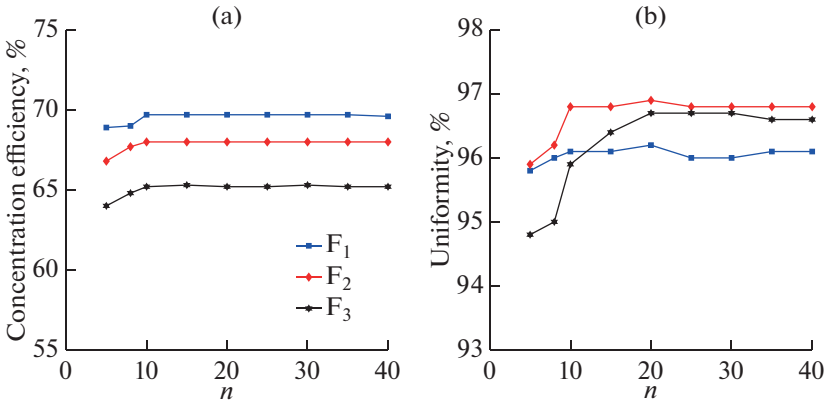

Fig. 4. Concentration efficiency (a) and uniformity (b) change with *n*.

equal *n* segments and the side of the laser crystal rod is also divided into *n* segments with same area. The focal length of each segment of the linear Fresnel lens is different, the sunlight converged by each segment of the linear Fresnel lens are distributed in a corresponding area on the side of the laser crystal rod, thus achieving a uniform distribution of the solar power on the side of the laser rod.

When the initial value of *n* is taken as 10, and the concentration efficiency of linear Fresnel lens F_1 is 69.7% with uniformity of 96.1% by ray-tracing; the concentration efficiency of linear Fresnel lens F_2 is 68% with uniformity of 96.8%; and the concentration efficiency of linear Fresnel lens F_3 is 65.2% with uniformity of 95.9%. In order to optimize the value of n, the *n* increases from 5 to 40 to discuss the linear Fresnel lenses F_1, F_2 and F_3 of the concentrating efficiency and light spot uniformity on the side of the laser crystal rod.

Figure 4 demonstrates that the concentration efficiency and uniformity change with *n*. The results show that the concentration efficiency of the linear Fresnel lens hardly changes when *n* increases from 10 to 40, and the fluctuation of uniformity does not exceed 1%, so the optimal value of *n* can be considered as 10.

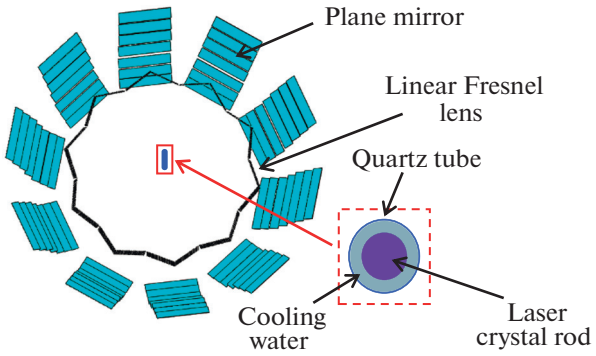

Fig. 5. The structure of the concentrating system.

Ultimately, the concentrating system of the solar-pumped solid-state laser consists of 10 subsystems. The laser head located in the center of the concentrating system, whose structure is shown in Fig. 5.

The effective area of the concentrating system receiving sunlight is 4.5 m^2, and the solar power collected on the laser crystal side is 2712.6 W. The sunlight passing through the quartz tube loses 68 W and the cooling water absorbs 243.2 W of solar power. The concentrating efficiency of the concentrating system and the uniformity are 66.5, and 98.5% from the information of irradiance, and the irradiance map of crystal side is shown in Fig. 6. The results show that the uniform distribution of the concentrating sunlight on the side of the laser crystal can be achieved.

THERMAL EFFECT ANALYSIS AND LASER OUTPUT POWER CALCULATION

For uniform pumping solar laser, the heat generated by the laser crystal rod is

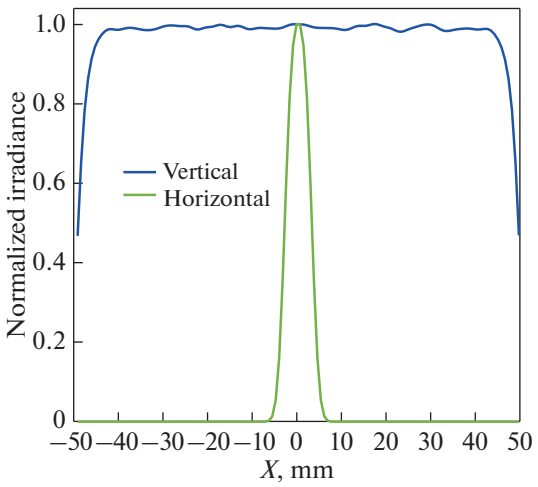

Fig. 6. Irradiance map of the side of the laser rod.

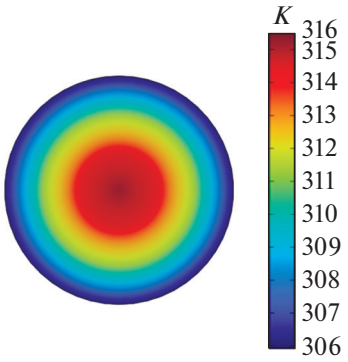

Fig. 7. Temperature distribution of laser rod cross-section.

$$Q_a = \eta_{heat}\eta_{ovp}\eta_a P. \quad (9)$$

Then, the heat generated per unit volume is

$$Q = \frac{Q_a}{\pi R^2 L}, \quad (10)$$

η_{heat} is the part of the absorbed pump power that converts into heat. η_{ovp} is the overlap of laser absorption spectra and solar spectra and η_a is the absorption efficiency. P is pumping power. L and R are the length and radius of the laser crystal rod, respectively. The temperature of cooling water is set to 20°C. The surface heat transfer coefficient, the heat load coefficient and the concentrated solar power on the laser crystal side are 0.69 W/cm^2 K, 0.46 [35] and 2712.6 W, respectively. The temperature distribution in the laser crystal rod is simulated by the Comsol software, and the result is shown in Fig. 7. The temperature is 306 K at the center of crystal rod end face and the surface temperature of crystal rod side is 316 K. The maximum thermal stress in the laser crystal rod is 10.5 MPa, which is 18.6 times lower than the maximum thermal stress of 195.3 MPa generated by end-pumping with same pumping power [36].

Nd:YAG is a typical four-level laser medium. Based on the rate equation [37], the laser output power is obtained as

$$P_{out} = \frac{2(1-R)\eta}{(1+R)(2\alpha l - \ln R)}\left(P_{in} - \frac{I_s(2\alpha l - \ln R)A}{2\eta}\right), \quad (11)$$

where $\eta = \eta_Q\eta_S\eta_B\eta_T\eta_{ovp}\eta_a$, the quantum efficiency (η_Q) [37], Stokes factor (η_S) [38], beam overlap efficiency (η_B) and transfer efficiency (η_T) are 0.9, 0.62, 0.91 and 0.85, respectively. The overlap between the absorption spectrum of the laser medium and the solar emission spectrum (η_{ovp}) is 0.16, and the absorption efficiency (η_a) is 0.837. η is 0.0566 and scattering coefficient α is 0.003 cm^{-1} for the 1.0 at % Nd:YAG [39]. I_s is the saturation intensity of the laser.

The size of Nd:YAG crystal rod is Φ 6 × 100 mm and the Nd dopant concentration is 1.0 at %. The relationship between laser output power and output cavity mirror reflectivity is shown in Fig. 8a. Figure 8b demonstrates the relationship between laser output power and pump solar power, and the pumping threshold is 668.1 W. The maximum laser output power reaches 88.5 W, and the slope efficiency and the solar-to-laser conversion efficiency are 4.3 and 3.3% when the output cavity mirror reflectivity of the resonant cavity is 83.5%.

CONCLUSIONS

The uniform side-pumping of solar laser can effectively reduce the thermal load on the laser crystal rod and obtain high power laser output. In this paper, the plane mirrors and the linear Fresnel lens array are used to design the solar concentrating system, which consists of ten subsystems. Ten subsystems are symmetrically distributed around the laser crystal rod. Each subsystem has seven layers of linear Fresnel lenses and

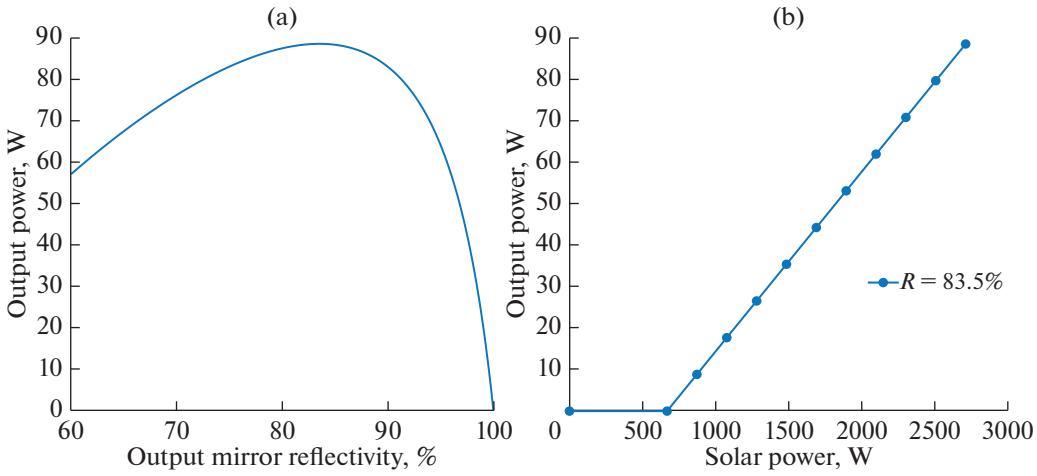

Fig. 8. Laser output power changes with the output cavity mirror reflectivity (a) and solar power (b).

plane mirrors. The incident sunlight is reflected by the plane mirrors and pass through the surface of the linear Fresnel lenses vertically. The other linear Fresnel lenses are symmetrical about the linear Fresnel lens F_0, which ensures that the concentrating sunlight is distributed uniformly along the axis of the laser crystal rod. The effective solar collection area of the concentrating system is 4.5 m^2, and 2712.6 W of solar power is collected on the side of the laser crystal rod. With the optimal design, the uniformity of sunlight power distribution on the laser crystal rod side and the concentrating efficiency of the concentrating system are 98.5 and 66.5%. The temperature distribution in the laser crystal rod is calculated by using Comsol software. The results shows that the highest temperature at the center of the laser rod end face is 316 K and the temperature of laser rod side is 306 K. Finally, by solving the rate equation, it is found that the laser output power is 88.5 W and the slope efficiency is 4.3%. Base on the linear Fresnel lens array, uniformly pumped solar laser is achieved, which provides a design method of solar concentrator for high-power solar pumped lasers.

FUNDING

The presented study is performed within Research Fund for Excellent Dissertation of China Three Gorges University (2021SSPY149).

CONFLICT OF INTEREST

The authors of this work declare that they have no conflicts of interest.

REFERENCES

1. Guan, Z., Zhao, C.M., Yang, S.H., Wang, Y., Ke, J.Y., and Zhang, H.Y., Demonstration of a free-space optical communication system using a solar-pumped laser as signal transmitter, *Laser Phys. Lett.,* 2017, vol. 14, no. 5, p. 055804. https://doi.org/10.1088/1612-202x/aa688a
2. Yabe, T., Uchida, S., Ikuta, K., Yoshida, K., Baasandash, C., Mohamed, M.S., Sakurai, Y., Ogata, Y., Tuji, M., Mori, Y., Satoh, Y., Ohkubo, T., Murahara, M., and Ikesue, A., Demonstrated fossil-fuel-free energy cycle using magnesium and laser, *Appl. Phys. Lett.,* 2006, vol. 89, no. 26, p. 261107. https://doi.org/10.1063/1.2423320
3. Zhu, J., Liu, Y., Lan, L., Tang, Y., Zhang, Y., and Ma, X., Solar side-pumped Nd-doped fiber laser based on a doughnut-shaped hollow reflector, *Laser Phys. Lett.,* 2023, vol. 20, p. 125101. https://doi.org/10.1088/1612-202X/ad0a70
4. Fazilov, A., Mansurov, M.M., and Abdurakhmanov, A.A., Calculated characteristics of the solar pumped solid-state laser, *Appl. Sol. Energy,* 2010, vol. 46, no. 3, pp. 228–231. https://doi.org/10.3103/S0003701X1003014X
5. Kiss, Z.J., Lewis, H.R., and Duncan, R.C., Sun pumped continuous optical maser, *Appl. Phys. Lett.,* 1963, vol. 2. no. 5, pp. 93–94. https://doi.org/10.1063/1.1753794
6. Sherniyozov, A.A. and Payziyev, S.D., Solar pumped lasers: High-efficiency multi-pass side pumping scheme with Fresnel lens, *Appl. Sol. Energy.,* 2020, vol. 56, no. 6, pp. 458–465. https://doi.org/10.3103/S0003701X20060092
7. Payziyev, S., Bakhramov, S., and Shayimov, F., Enhancing of solar pumped liquid laser efficiency, *Appl. Sol. Energy.,* 2016, vol. 52, no. 1, pp. 68–71. https://doi.org/10.3103/S0003701X16010096
8. Payziyev, S., Makhmudov, K., Bakhramov, S., Sherniyozov, A., and Zikrillayev, K., Solar-pumped multi-rod laser on a separate heliostat of big solar furnace, *Appl. Sol. Energy,* 2021, vol. 57, no. 6, pp. 541–551. https://doi.org/10.3103/S0003701X2106013X
9. Wang, B., Lan, L., Liu, Y., Tang, Y., and Zhang, Y., Investigation of a 100W solar-pumped disk laser with TEM00 output, *J. Russ. Laser Res.,* 2023, vol. 44, no. 6, pp. 682–690. https://doi.org/10.1007/s10946-023-10178-y
10. Falk, J., Huff, L., and Taynai, J.D., Solar-pumped, mode-locked, frequency-doubled Nd:YAG, *IEEE J. Quant. Electron.,* 1975, vol. 11, no. 9, pp. 836–837. https://doi.org/10.1109/JQE.1975.1068930
11. Cooke, D., Sun-pumped lasers: Revisiting an old problem with nonimaging optics, *Appl. Opt.,* 1992, vol. 31, no. 36, pp. 7541–7546. https://doi.org/10.1364/ao.31.007541
12. Yabe, T., Ohkubo, T., Uchida, S., Yoshida, K., Bagheri, B., Funatsu, T., Mabuti, A., Oyama, A., Nakagawa, K., Oishi, T., Daito, K., Nakatsuka, M., Yoshida, M., Motokoshi, S., Sato, Y., Baasandash, C., Nakayama, N., Okamoto, Y., and Yanagaidani, K., Experimental study of solar pumped laser for magnesium-hydrogen energy cycle, *J. Phys.: Conf. Ser.,* 2008, vol. 112, p. 042072. https://doi.org/10.1088/1742-6596/112/4/042072
13. Ou, M.Y., Hu, P., Lan, L.L., Liu, Y., Zhou, J., and Shi, X.T., Design of a Fresnel lens for a solar end-pumped solid-state laser, *Curr. Opt. Photonics.,* 2020, vol. 4, no. 5, pp. 441–445. https://doi.org/10.3807/COPP.2020.4.5.441
14. Mehellou, S., Rehouma, F., Hamrouni, N., and Bouras, L., Thermal loading effects on Nd:YAG solar-laser performance in end-pumping and side-pumping configurations: a review, *Opt, Eng.,* 2018, vol. 57, no. 12, p. 120902. https://doi.org/10.1117/1.OE.57.12.120902
15. Hamrouni, N., Mehellou, S., and Rehouma, F., Study of Nd:YAG solar laser output performance in end-pumping and side pumping, *J. Fundam. Appl. Sci.,* 2020, vol.12, pp. 49–55. https://doi.org/10.4314/jfas.v12i1S.4
16. Mehellou, S., Beggas, A., Herrmrouni, N., and Rehouma, F., The effects of the pumping configurations on TEM00 mode Nd:YAG solar laser performance: A review, *Braz. J. Phys.,* 2022, vol. 52, p. 169. https://doi.org/10.1007/s13538-022-01163-y
17. Lando, M., Kagan, J., Linyekin, B., and Dobrusin, V., A solar-pumped Nd:YAG laser in the high collection

efficiency regime, *Opt. Commun.,* 2003, vol. 222, nos. 1–6, pp. 371–381. https://doi.org/10.1016/S0030-4018(03)01601-8

18. Dinh, T.H., Ohkubo, T., Yabe, T., and Kuboyama, H., 120 Watt continuous wave solar-pumped laser with a liquid light-guide lens and an Nd:YAG rod, *Opt. Lett.,* 2012, vol. 37, no. 13, pp. 2670–2672. https://doi.org/10.1364/OL.37.002670

19. Xu, P., Yang, S.H., Zhao, C.M, Guan, Z., Wang, H.X., Zhang, Y.C., Zhang, H.Y., and Tao He, T., High-efficiency solar-pumped laser with a grooved Nd:YAG rod, *Appl. Opt.,* 2014, vol. 53, no. 18, pp. 3941–3944. https://doi.org/10.1364/AO.53.003941

20. Almeida, J., Liang, D., Vistas, C.R., Bouadjemine, R., and Guillot, E., 5.5W TEM00-mode Nd:YAG solar laser by a light guide/2V pump cavity, *Appl. Phys. B,* 2015, vol. 121, pp. 473–482. https://doi.org/10.1007/s00340-015-6257-z

21. Mehellou, S., Dawei Liang, D., Joana Almeida, J., Rochdi Bouadjemine, R., R. Vistas, C., Em-manuel Guillot, and Rehouma, F., Stable solar-pumped TEM00-mode 1064 nm laser emission by a monolithic fused silica twisted light guide, *Sol. Energy,* 2017, vol. 155, pp. 1059–1071. https://doi.org/10.1016/j.solener.2017.07.048

22. Vistas, C.R., Liang, D., Garcia, D., Tiburcio, B.D., and Almeida, J., 32 W TEM00-Mode side-pumped solar laser design, *Appl. Sol. Energy,* 2020, vol. 56, no. 6, pp. 449–457. https://doi.org/10.3103/S0003701X20060122

23. Boutaka, R., Liang, D., Bouadjemine, R., Traiche, M., and Kellou, A., A compact solar laser side-pumping scheme using four off-axis parabolic mirrors, *J. Russ. Laser Res.,* 2021, vol. 42, no. 4, pp. 453–461. https://doi.org/10.1007/s10946-021-09982-1

24. Guo, P., Zhang,J.M., Chen, Z., Lan, L.L., Liu, Y., Tang, Y.L., and Ma, X.H., Side-pumped solar Nd-doped fiber laser based on off-axis parabolic mirror array, *Optik,* 2022, vol. 271, p. 170096. https://doi.org/10.1016/j.ijleo.2022.170096

25. Endo, M., Bisson, J.F., and Masuda, T., Monte Carlo simulation of a transversely excited solar-pumped fiber laser, *Jpn. J. Appl. Phys.,* 2019, vol. 58, no. 11, p. 112006. https://doi.org/10.7567/1347-4065/ab4a93

26. Xiang, P.F., Lan, L.L., Liu, Y., Qi, H.F., Tang, Y.L., and Ma, X.H., Theoretical analysis of a 60 W solar-pumped single crystal fiber laser, *Appl. Opt.,* 2022, vol. 61, no. 30, pp. 8988–8993. https://doi.org/10.1364/AO.471537

27. Vistas, C.R., Liang, D., Almeida, J., Tibúrcio, B.D., Garcia, D., Catela, M., Costa, H., and Guillot, E., Ce:Nd:YAG side-pumped solar laser, *J. Photonics Energy,* 2021, vol. 11, no. 1, p. 018001. https://doi.org/10.1117/1.JPE.11.018001

28. Almeida, J., Liang, D., Garcia, D., Tibúrcio, B.D., Costa, H., Catela, M., Guillot, E., and Vistas, C.R., 40 W continuous wave Ce:Nd:YAG solar laser through a fused silica light guide, *Energies,* 2022, vol. 15, no. 11, p. 3998. https://doi.org/10.3390/en15113998

29. Garcia, D., Liang, D., Vistas, C.R., Costa, H., Catela, M., Tibúrcio, B.D., and Almeida, J., Ce:Nd:YAG solar laser with 4.5% solar-to-laser conversion efficiency, *Energies,* 2022, vol. 15, no. 14, p. 5292. https://doi.org/10.3390/en15145292

30. Liang, D., Vistas, C.R., Garcia, D., Tibúrcio, B.D., Catela, M., Costa, H., Guillot, E. and Almeida, J., Most efficient simultaneous solar laser emissions from three Ce:Nd:YAG rods within a single pump cavity, *Sol. Energy Mater. Sol. Cells,* 2022, vol. 246, p. 111921. https://doi.org/10.1016/j.solmat.2022.111921

31. Cai, Z., Zhao, C.M., Zhao, Z.Y., Zhang, J., Zhang, Z.L. and Zhang, H.Y., Efficient 38.8 W/m^2 solar pumped laser with a Ce:Nd:YAG crystal and a Fresnel lens, *Opt. Express.,* 2023, vol. 31, no. 2, pp. 1340–1353. https://doi.org/10.1364/OE.481590

32. Liang, D. and Almeida, J., Multi-Fresnel lenses pumping approach for improving high-power Nd:YAG solar laser beam quality, *Appl. Opt.,* 2013, vol. 52, no. 21, pp. 5123–5132. https://doi.org/10.1364/AO.52.005123

33. Wang, J.J., Wang X. and Ning, D., Off-axis non-rotationally symmetric superposition square spot uniform concentration Fresnel lens, *Acta Photonica Sin.,* 2017, vol. 46, no. 6, p. 0622003. https://doi.org/10.3788/gzxb20174606.0622003

34. Yang, S.H, Xu, P., Zhao,C.M., Guan, Z., Wang, H.X., Zhang, Y.C., Zhang, H.Y., and He, T., 28W Solar-pumped laser with a grooved Nd:YAG rod, in *Proc. Advanced Solid State Lasers 2014, Shanghai,* 2014, p. ATU2A.45. https://doi.org/10.1364/ASSL.2014.ATu2A.45

35. Zhao, C.M., *Solar Pumped Lasers,* Beijing: Nation Defense Industry Press, 2016.

36. Matos, R., Liang, D., Almeida, J., Tibúrcio, B.D., and Vistas, C.R., High-efficiency solar laser pumping by a modified ring-array concentrator, *Opt. Commun.,* 2018, vol. 420, pp. 6–13. https://doi.org/10.1016/j.optcom.2018.03.027

37. Koechner, W., *Solid-State Laser Engineering,* Berlin: Springer-Verlag, 1999.

38. Weksler, M. and Shwartz, J., Solar-pumped solid-state lasers, *IEEE J. Quantum Electron.,* 1988, vol. 24, no. 6, pp. 1222–1228. https://doi.org/10.1109/3.247

39. Almeida, J., Liang, D., Vistas C.R., and Guillot, E., Highly efficient end-side-pumped Nd:YAG solar laser by a heliostat-parabolic mirror system, *Appl. Opt.,* 2015, vol. 54, no. 8, pp. 1970–1977. https://doi.org/10.1364/AO.54.001970